TOXICOLOGICAL SCIENCES **94(2)**, 359–367 (2006)
doi:10.1093/toxsci/kfl112
Advance Access publication September 19, 2006

Use of a Pharmacokinetic-Driven Computational Fluid Dynamics Model to Predict Nasal Extraction of Hydrogen Sulfide in Rats and Humans

Jeffry D. Schroeter,[1] Julia S. Kimbell, Melvin E. Andersen, and David C. Dorman

CIIT Centers for Health Research, Research Triangle Park, North Carolina 27709-2137

Received July 18, 2006; accepted September 17, 2006

Hydrogen sulfide (H_2S) is a naturally occurring and industrially generated gas. Human exposure to H_2S results in dose-related neurological, respiratory, and cardiovascular effects. Subchronic exposure of rats to 30 or 80 ppm H_2S results in olfactory neuron loss and basal cell hyperplasia. Olfactory lesions commonly border main airflow streams in the rat, indicating an influence of airflow on H_2S-induced lesion locations. In this study, anatomically accurate computational fluid dynamics (CFD) models were used to quantitatively predict H_2S tissue dose in rat and human nasal passages. Air-tissue flux was defined in terms of H_2S solubility, diffusivity, and reaction kinetics in nasal tissue. Kinetic parameters for the rat were estimated from an air-tissue pharmacokinetic (PK) model that was fit to experimental nasal extraction (NE) data. Using this PK-driven CFD model, predicted flux at the mid-dorsomedial meatus and the middle portion of the ethmoid recess showed a good correlation with olfactory lesion incidence. Scaled kinetic parameters were incorporated into a human CFD model to predict H_2S flux in human nasal passages. Assuming that equivalent H_2S flux values will induce similar responses in the olfactory regions of rats and humans, a no-observed-adverse-effect–level human-equivalent concentration was estimated to be 5 ppm. This estimate was based on quantitative tissue dose estimates extrapolated from both lesion and NE data in rats and represents a risk estimate that is science based and does not rely on simplified dosimetric assumptions for interspecies extrapolation.

Key Words: **hydrogen sulfide; computational fluid dynamics; pharmacokinetics; olfactory; nasal passages; interspecies extrapolation.**

Hydrogen sulfide (H_2S) is a naturally occurring toxic gas found in petroleum, natural gas, and volcanic and sulfur spring emissions. H_2S is also released into the environment as a by-product of various industrial processes, including sewage treatment, pulp and paper processing, and petroleum and natural gas drilling and refining operations (ATSDR, 1999). While exposure to high concentrations of H_2S is typically associated with confined exposures in an occupational setting, human exposure to low levels of H_2S is widespread due to its prevalence in the environment. The severity of adverse effects progresses with increased H_2S exposure level and duration (Beauchamp *et al.*, 1984; Glass, 1990; Reiffenstein *et al.*, 1992), and predominantly affects the nervous, cardiovascular, and respiratory systems (ATSDR, 1999).

The olfactory epithelium is particularly vulnerable to H_2S-induced pathology and has formed the basis for occupational and environmental exposure standards. Subchronic exposure of rats and mice to 30 or 80 ppm H_2S resulted in olfactory neuron loss and basal cell hyperplasia on the dorsal medial meatus and the dorsal and medial aspects of the ethmoid recess (Brenneman *et al.*, 2000; Dorman *et al.*, 2004). Acute exposure of rats to $\geq$ 80 ppm resulted in full thickness necrosis of the olfactory mucosa on the dorsal meatus (Brenneman *et al.*, 2002; Lopez *et al.*, 1988). Decreased cytochrome oxidase activity and increased tissue sulfide concentrations were observed following acute exposure to 80 and 400 ppm H_2S, respectively (Dorman *et al.*, 2002; Roberts *et al.*, 2006), indicating that inhibition of cytochrome oxidase may be a likely mode of action for toxicity.

Olfactory pathology induced by H_2S inhalation commonly border regions where airflow velocity may be relatively high in the nasal passages, indicating that high flux of H_2S into nasal tissue may contribute to olfactory lesions. To test this hypothesis, computational fluid dynamics (CFD) models have been developed to describe the uptake of inhaled H_2S in rat nasal passages (Moulin *et al.*, 2002; Schroeter *et al.*, 2006). Moulin and colleagues (2002) used the nasal airflow model developed by Kimbell *et al.* (1997a) to predict olfactory regions that received high H_2S flux during inspiratory flow. These simulations showed a good correlation between areas of high flux on airway walls with olfactory epithelial responses in the rat nasal cavity. However, since nasal extraction (NE) efficiency of H_2S was unknown, these correlations were only qualitative and were unable to quantify the amount of H_2S absorbed by nasal tissues.

Subsequently, H_2S NE was measured in the isolated upper respiratory tracts of anesthetized rats under steady inspiratory

[1] To whom correspondence should be addressed at CIIT Centers for Health Research, 6 Davis Drive, PO Box 12137, Research Triangle Park, NC 27709-2137. Fax: 919-558-1300. E-mail: jschroeter@ciit.org.

flow (Schroeter *et al.*, 2006). Extraction efficiency was fairly low (< 35%) at a 10-ppm exposure level and decreased further as H_2S exposure concentration increased. These extraction data were used to estimate kinetic parameters governing systemic and metabolic clearance in nasal tissue with a pharmacokinetic (PK) model. The estimated kinetic parameters were then implemented in a boundary condition for the CFD model that incorporated first-order and saturable tissue reaction kinetics in nasal tissue to govern mass flux at the air-tissue interface. Extraction of H_2S in rat nasal passages predicted with this PK-driven CFD model compared well with the experimental data.

In this study, the PK-driven CFD model developed by Schroeter *et al.* (2006) was used to compare regions of high-predicted H_2S flux in rat nasal passages with the distribution of H_2S-induced olfactory lesions from a subchronic H_2S inhalation study (Brenneman *et al.*, 2000), in a manner similar to Moulin *et al.* (2002). Since this model yields a quantitative flux measure, we were able to estimate the minimum flux value associated with olfactory lesions in rats. This modeling approach was then used to predict H_2S flux in human nasal passages by scaling the kinetic parameters and implementing a similar boundary condition in a human nasal airflow model (Subramaniam *et al.*, 1998). Olfactory flux levels predicted from the human CFD model were used to derive a no-observed-adverse-effect–level human-equivalent concentration ($NOAEL_{[HEC]}$) for H_2S. This $NOAEL_{[HEC]}$ value can be used as a guide in establishing an inhalation reference concentration (RfC) (U.S. EPA, 1994).

METHODS

Computational nasal airflow models have been previously developed to predict airflow patterns and regions of high wall mass flux of inhaled chemicals in the upper respiratory tracts of various species (Kepler *et al.*, 1998; Keyhani, 1997; Kimbell *et al.*, 1993, 1997a,b; 2001a,b; Scherer *et al.*, 1994). The model developed by Schroeter *et al.* (2006) to study uptake of inhaled H_2S in rat nasal passages incorporated tissue dosimetry and saturable PK processes, thereby expanding the scope of gas uptake models beyond the air phase to include tissue phase transport mechanisms. This PK-driven CFD model was used in this study to identify regions of high wall mass flux and to quantitatively obtain tissue dose estimates in the olfactory region of the rat nasal cavity. In the following sections, the rat and human nasal airflow models are described, along with the correlation of flux predictions with olfactory lesion incidence and the interspecies scaling of the kinetic parameters from rats to humans.

Nasal airflow models. Rat nasal airflow simulations were conducted with the CFD model developed by Kimbell and colleagues (1997a). This model is an anatomically accurate 3-D reconstruction of the right nasal passages of a mature F344 rat from tracings of serial histological cross-sections. Airflow in the human nasal passages was simulated with the CFD model developed by Subramaniam and colleagues (1998). This model was reconstructed from MRI scan tracings of the nasal passages of a healthy, nonsmoking adult male. Since inhaled H_2S is known to affect the olfactory system, the olfactory regions in the rat and human nasal cavities were identified in the CFD models (Fig. 1).

The computational meshes for the rat and human nasal models were formed from structured hexahedral elements resulting in approximately 144,000 and 156,000 nodes, respectively. A no-slip boundary condition was implemented on all airway walls, a stress-free condition was imposed at the outlet, and a uniform velocity profile was defined at the nostrils. The Navier-Stokes equations governing viscous incompressible flow were solved with the finite element method using FIDAP (Fluent, Inc., Lebanon, NH). Airflow simulations were conducted at steady state in the inspiratory direction. Predicted flow patterns compared well with dye-streakline visualizations and published observations (Kimbell *et al.*, 1993; Kimbell *et al.*, 1997a; Subramaniam *et al.*, 1998).

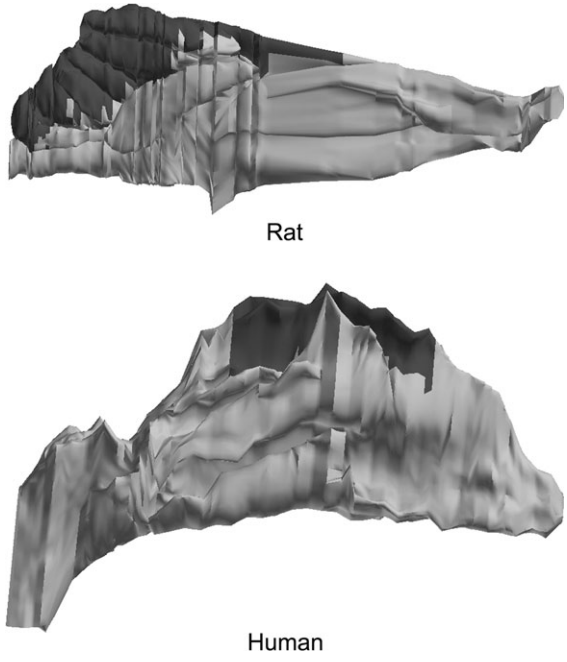

FIG. 1. Lateral view of the rat and human nasal airflow models (gray) with their corresponding olfactory regions (black). The nostrils are to the right, and the nasopharynxes are to the left. The surface areas for the olfactory regions are 7.6 and 23.4 cm^2 for the rat and human models, respectively.

To be comparable across species, inspiratory flow rates were calculated by dividing the amount of inspired air (tidal volume) by the estimated time involved in inhalation (half the time of one breath). Therefore, a steady inspiratory flow rate was calculated to be twice the minute volume. The inspiratory flow rate for the rat was 576 ml/min, derived from a minute volume that was allometrically scaled to 288 ml/min for a 315-g rat (Mauderly, 1986). Human inspiratory flow was estimated to be 13.8 l/min, based on a 70-kg human inhaling 20 m^3/day (U.S. EPA, 1994). The associated Reynolds numbers (ratio of inertial to viscous forces) at the nostrils were 241 and 671 for the rat and human, respectively.

Predicted H_2S uptake. Transport and dosimetry of inhaled H_2S in the nasal passages were governed by convection of inhaled air and molecular diffusion onto airway walls. At low concentrations, the presence of H_2S was assumed to have no effect on airflow behavior, so the solution of the convection-diffusion equation was decoupled from the airflow simulations and solved as a secondary step with FIDAP (Fluent, Inc., Lebanon, NH). The concentration of inhaled H_2S was specified at the nostrils, and a mass transfer term defining diffusive flux to the airway walls was specified on all epithelial surfaces. The standard form for this boundary condition relates flux at the airway walls with concentration near the walls and is written as

$$\text{flux} = hC_{\text{air}},$$

where h is referred to as the air phase mass transfer coefficient and C_{air} is the concentration of H_2S near the airway walls.

For constant values of h, this form of boundary condition will predict constant extraction efficiency, regardless of exposure concentration. Therefore, the air phase mass transfer coefficient was modified to account for the observed

concentration dependence of H_2S NE (Schroeter *et al.*, 2006). A tissue layer lining the air phase of the CFD model was implemented so that flux of H_2S onto the air-tissue interface was governed by tissue diffusion and reaction kinetics. The air phase mass transfer coefficient (h) was computed based on the equilibrium assumption at the air-tissue interface. In this manner, flux from the air phase incorporated H_2S solubility, diffusivity in nasal tissue, a first-order rate constant (k_f) representing systemic and local metabolic clearance, and Michaelis-Menten constants (V_{max} and K_m) governing saturable clearance processes. The kinetic parameters k_f, V_{max}, and K_m were estimated by fitting NE predicted by an air-tissue PK model to time-averaged NE data (Schroeter *et al.*, 2006).

Correlation of flux predictions with lesion locations in the rat. In a previous study, adult male CD rats were subchronically exposed to 0, 10, 30, or 80 ppm H_2S, and their nasal cavities were histologically evaluated for exposure-related lesions (Brenneman *et al.*, 2000). Transverse cuts were made perpendicular to the bridge of the nose at five sites, resulting in six tissue blocks. Subsequently, two sections were selected at the approximate midpoint of the nasal cavity and the middle portion of the ethmoid recess (Moulin *et al.*, 2002) because they contain olfactory epithelium and were affected by H_2S exposure (Fig. 2). Lesion severity in both sections was subjectively graded by visual estimation of the average percentage of the normal olfactory neuronal cell layer altered by H_2S exposure and was rated as mild (26–50%), moderate (51–75%), or severe (76–100%). The portion of the airway perimeters lined with olfactory epithelium was further divided into regions based on anatomical landmarks with each segment of approximately the same length (300–1000 μm) (Fig. 2). The presence of olfactory lesions that were at least moderately severe was determined in all regions of both sections. Changes in the olfactory mucosa with similar incidence and severity as those found in control groups were regarded as background findings and were excluded from the analysis.

Transverse cross-sections corresponding to sections 1 and 2 for the nasal pathology were identified in the rat nasal airflow model. The perimeters of these sections were divided into regions that contain olfactory epithelium and were identical to the regions identified for recording of lesion incidence. Average H_2S flux in each of these regions was computed with the CFD model. Average flux and lesion incidence in each region were ranked and a correlation between the two data sets was determined using Spearman's rank correlation coefficient, a technique used to describe the strength of a rank order relationship between two sets of data (Mendenhall *et al.*, 1981).

Parameter scaling. To predict extraction of H_2S in human nasal passages, the PK parameters describing tissue clearance processes in the rat were scaled to account for different metabolic rates between rats and humans. A common approach in PKs to account for differences in pulmonary physiology and general metabolism is to assume an allometric relationship of the form $Y = a(BW)^b$, where BW is body weight and a and b are empirical constants (Krishnan and Andersen, 1991). Since the metabolic characteristics of H_2S are unknown in other species, there is no experimental basis to derive these constants for this study. Therefore, as a starting point, an allometric relationship was used that has been established for interspecies scaling of styrene liver clearance (Ramsey and Andersen, 1984). A value of 0.7 was selected for the exponent as a compromise between body surface area (0.67) and blood flow rate (0.75) scaling (Mordenti and Chappell, 1989). However, since this study was concerned with NE, the derived interspecies scaling parameter was further corrected for the relative nasal surface areas per body weight between rats and humans (Mahmood, 2001). Applying this anatomically based correction factor that accounts for nasal epithelial surface area differences, the interspecies scaling factor for metabolic rate per unit mass, $\lambda_{R:H}$, can be written as

$$\lambda_{R:H} = \left(\frac{BW^H}{BW^R}\right)^{0.7} \bullet \frac{\{\text{nasal surface area per BW}\}^H}{\{\text{nasal surface area per BW}\}^R}.$$

This scaling factor was applied to the first-order rate constant for clearance, k_f, and the maximal metabolic rate, V_{max}. The Michaelis-Menten parameter K_m and the air-tissue partition coefficients were assumed to be species invariant (Table 1).

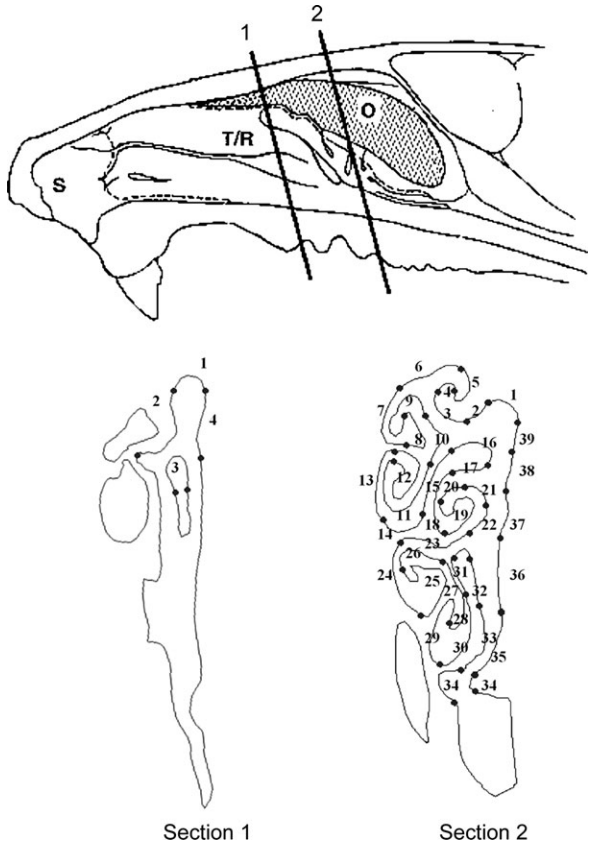

FIG. 2. Top: Schematic of the nasal mucosa with the two section levels used to evaluate nasal pathology. Bottom: The perimeters of the olfactory epithelium in sections 1 and 2 were divided into 4 and 39 regions, respectively. The regions were consecutively numbered with region 1 located at the roof of the dorsal medial meatus. Reproduced from Moulin *et al.* (2002) by permission of the Society of Toxicology.

RESULTS

Olfactory Lesion Incidence

A description of the nasal lesions found in CD rats following subchronic exposure to H_2S has been described in detail

TABLE 1
Model Parameters and Kinetic Constants used in the Rat and Human H_2S CFD Models

	Rat	Human
Body weight (kg)	0.315	70
Nasal surface area (mm^2)	1851	24,611
Nasal tissue thickness (μm)	84	375
Minute volume (l/min)	0.288	6.9
H_2S tissue:air partition coefficient	2.8	2.8
V_{max} (μmol/min)	183.8	477.9[a]
K_m (μmol/ml)	27.7	27.7
k_f (min^{-1})	5.3	13.8[a]

[a]allometrically scaled from the rat.

(Brenneman *et al.*, 2000; Moulin *et al.*, 2002). Briefly, nasal lesions limited to the olfactory mucosa were observed following exposure to 30 or 80 ppm H_2S and consisted of multifocal, bilaterally symmetric olfactory neuron loss and basal cell hyperplasia. The incidence, mean severity, and distribution of olfactory lesions increased with exposure concentration, affecting approximately 50 and 70% of the olfactory epithelium at exposure concentrations of 30 and 80 ppm H_2S, respectively. In section 1, olfactory epithelium was present on the dorsal medial meatus and the dorsal aspect of the third ethmoturbinate. An increased lesion incidence occurred at all these sites following exposure to 30 or 80 ppm H_2S (Table 2, Fig. 3A). In section 2, olfactory epithelium lined most of the nasal cavity, except for the ventral meatus and parts of the lateral walls, which were lined by respiratory epithelium. Nevertheless, H_2S-induced lesions were found only in specific sites on the olfactory epithelium, including the nasal septum, the dorsal walls of the nasal cavity, and the margins of the ethmoturbinates (Table 3, Fig. 4A). No lesions were observed following exposure to 10 ppm H_2S.

Predicted H_2S Dosimetry in Rat Nasal Passages

Airflow in the rat nasal passages was simulated with the CFD model at a steady-state volumetric inspiratory flow rate of 576 ml/min. The mass transfer boundary condition that relates air phase flux to tissue diffusion and clearance processes was implemented with the kinetic parameters estimated by Schroeter *et al.* (2006) (Table 1). Inlet concentrations of 10, 30, and 80 ppm were defined at the nostril to correlate with the exposure concentrations used in the subchronic inhalation study described above (Brenneman *et al.*, 2000).

Predicted H_2S flux across the air-tissue interface was computed in each region in sections 1 and 2 (Figs. 3B and 4B). In all regions, H_2S flux increased with increasing exposure concentration, although the rate of increase slowed as concentration increased due to the saturable nature of H_2S extraction. In section 1, the highest flux values occurred on the lateral wall of the dorsal medial meatus (region 2), with maximum flux values of 82, 34, and 12 pmol/cm^2·s at concentrations of 80, 30, and 10 ppm, respectively (Table 2, Fig. 3B). In section 2, the highest flux values were predicted to occur on the laterodorsal aspect of the dorsal medial meatus (region 2), the medial aspects of the third ethmoturbinate (regions 16 and 21), the medial aspect of the fifth ethmoturbinate (regions 32 and 33), and the mid-to-dorsal septum (regions 36–39). The maximum flux occurred in region 2, with maximum flux values of 249, 96, and 34 pmol/cm^2·s at 80, 30, and 10 ppm, respectively (Table 3, Fig. 4B).

TABLE 2
Predicted H_2S Flux and Nasal Lesion Incidence for Section 1

	Predicted flux (pmol/cm^2·s)			Lesion incidence (%)	
Region number	10	30	80	30	80
1	10.7	30.5	72.5	17	83
2	12.1	34.4	82.0	83	100
3	9.6	27.3	65.1	14	63
4	10.8	30.7	73.0	83	100

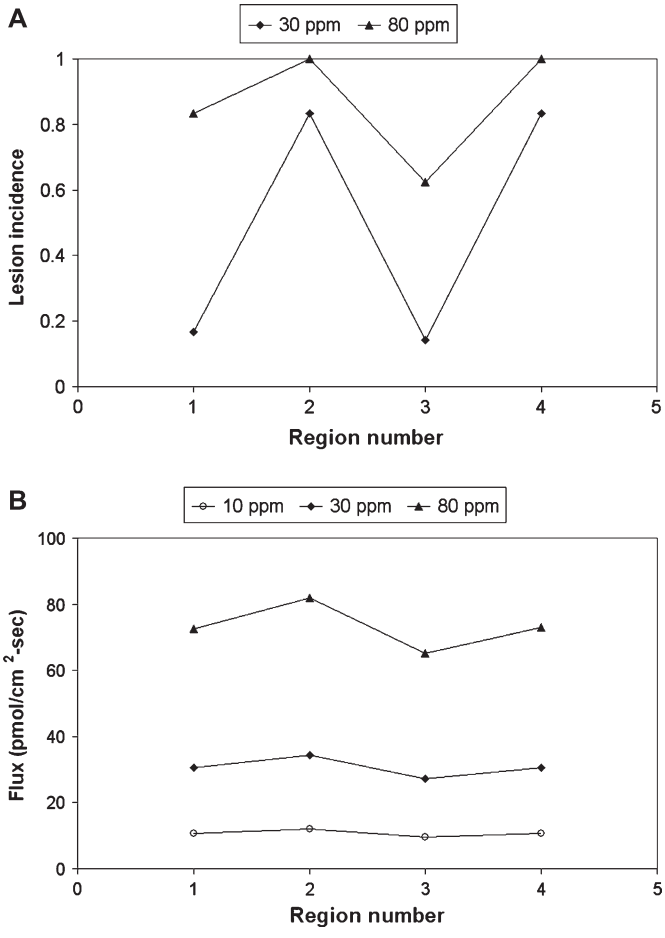

FIG. 3. (A) Lesion incidence at 30 and 80 ppm H_2S exposure in section 1. (B) Predicted H_2S flux from the CFD model at 10, 30, and 80 ppm exposure conditions in section 1.

Comparison of Flux Predictions and Olfactory Lesion Incidence

In section 1, a rank correlation coefficient could not be computed due to the small number of regions. However, it can be observed that for both the 30- and 80-ppm exposures, predicted flux increased or decreased accordingly with lesion incidence (Fig. 3).

In section 2, a significant correlation ($p < 0.05$) was found between H_2S flux and lesion incidence. At 30 ppm, the rank correlation coefficient was computed to be 0.53 with a p value of 0.0007, and at 80 ppm, the rank correlation coefficient was 0.60 with a p value of 0.0001. At 30 ppm, olfactory lesions only occurred in regions 2, 16, 17, 21, and 37–39. These regions were also predicted to receive the highest flux values

TABLE 3
Predicted H_2S Flux and Nasal Lesion Incidence for Section 2

	Predicted flux (pmol/cm^2·s)			Lesion incidence (%)	
Region number	10	30	80	30	80
1	10.5	29.9	71.8	0	67
2	33.8	96.3	248.9	45	92
3	3.3	10.5	25.9	0	29
4	12.4	36.1	96.0	0	0
5	5.1	15.2	40.2	0	14
6	8.1	24.4	63.8	0	33
7	5.1	15.8	41.6	0	13
8	2.9	9.4	24.7	0	13
9	4.5	13.8	35.9	0	11
10	9.4	27.3	69.6	0	78
11	2.4	8.2	20.6	0	0
12	2.5	8.6	22.3	0	0
13	2.6	8.7	22.5	0	11
14	2.7	8.2	20.6	0	13
15	5.3	16.0	40.6	0	67
16	22.5	64.2	164.7	75	100
17	10.6	30.3	73.6	18	75
18	4.2	12.3	28.9	0	33
19	7.1	21.1	53.9	0	13
20	10.9	31.4	78.6	0	42
21	14.4	41.2	101.4	27	92
22	10.8	30.8	74.5	0	50
23	−1.6	−6.0	−17.0	0	0
24	5.9	18.4	48.5	0	0
25	−4.4	−13.2	−36.8	NA	NA
26	−2.7	−8.9	−24.4	0	0
27	4.6	14.1	35.2	0	0
28	6.3	18.7	48.4	NA	NA
29	7.2	21.6	55.4	NA	NA
30	0.4	1.5	2.5	0	0
31	3.2	9.0	20.2	0	33
32	17.7	50.7	125.5	0	0
33	22.4	64.8	166.7	0	NA
34	−1.1	−1.1	−7.5	NA	NA
35	4.0	11.5	23.7	NA	NA
36	9.4	26.9	64.7	0	83
37	10.2	29.0	69.9	17	100
38	9.7	27.8	66.0	25	92
39	10.5	30.0	71.8	50	92

Note. NA, not applicable.

(> 28 pmol/cm^2·s) at this concentration. At 80 ppm, regions 2, 10, 16, 17, 21, and 36–39 recorded the greatest lesion incidence (> 75%) and, with the exception of region 10, coincided with the regions that recorded lesions at 30 ppm. These regions were also associated with the highest predicted flux values (> 65 pmol/cm^2·s) at this concentration. No lesions were recorded at 10 ppm, and with the exception of region 2, all regions were predicted to receive low flux (< 23 pmol/cm^2·s).

Predicted H_2S Dosimetry in Human Nasal Passages

Airflow simulations in the human nasal passages were conducted at a volumetric flow rate of 13.8 l/min. The mass

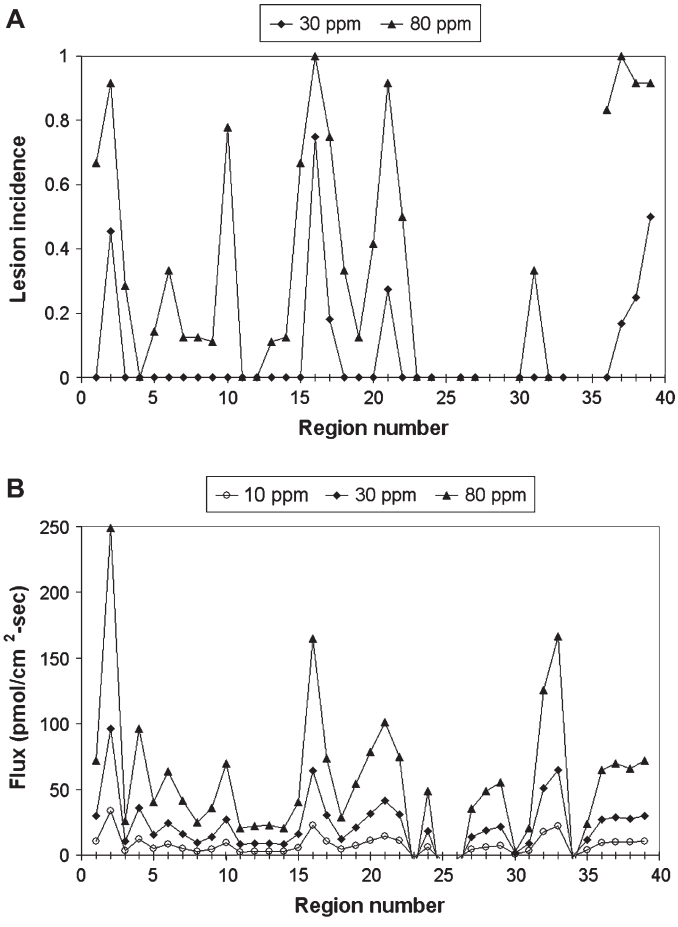

FIG. 4. (A) Lesion incidence at 30 and 80 ppm H_2S exposure in section 2. (B) Predicted H_2S flux from the CFD model at 10, 30, and 80 ppm exposure conditions in section 2. Nasal lesion data were not available in regions 25, 28, 29, 34, and 35 at the 30-ppm exposure and, in addition, for region 33 at the 80-ppm exposure. Negative flux values were predicted by the CFD model for region numbers 23, 25, 26, and 34 at all exposure concentrations (most likely due to numerical errors associated with the nonlinear boundary condition); these data points are not shown.

transfer term defining flux at the air-tissue interface was computed with the kinetic parameters scaled to the human (Table 1). Applying the allometric scaling by body weight raised to the 0.7 power yields a scaling factor of 45. With the nasal surface area per body weight correction, the final metabolic scaling factor used was $\lambda_{R:H} = 2.6$. H_2S uptake simulations were conducted with the human nasal CFD model by defining the appropriate inlet concentrations at the nostrils.

Predicted wall mass flux was compared in the rat and human nasal passages at 10 and 30 ppm exposure concentrations (Fig. 5). At 10 ppm, high flux regions in the human nose were visible in parts of the posterior olfactory region and the nasopharynx. A similar pattern held for the 30-ppm simulation, with high flux values covering a greater area in the olfactory region and nasopharynx and slightly higher fluxes throughout the nose. Significantly higher fluxes were predicted in the rat nasal passages. At 10 ppm, high flux values were visible in the

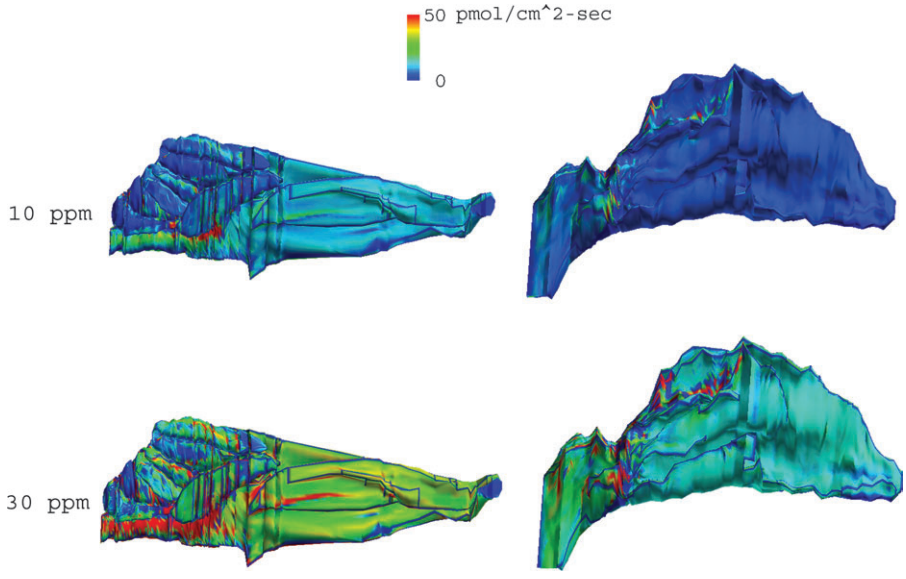

FIG. 5. Lateral view of wall mass flux of inhaled H_2S in the rat and human nasal passages at steady-state inspiratory flow rates of 576 ml/min and 13.8 l/min, respectively, at exposure concentrations of 10 and 30 ppm.

nasopharynx. At 30 ppm, there was a more uniform distribution of moderately high flux values, with higher fluxes reported in parts of the olfactory region and the nasopharynx.

Further H_2S uptake simulations were conducted in the human nasal passages at various exposure concentrations between 1 and 50 ppm. The maximum and 99th percentile flux values were computed for the human olfactory region at each concentration level (Fig. 6). Average olfactory flux values were also computed (data not shown) and were approximately 10 times smaller than the maximum olfactory flux at each exposure concentration.

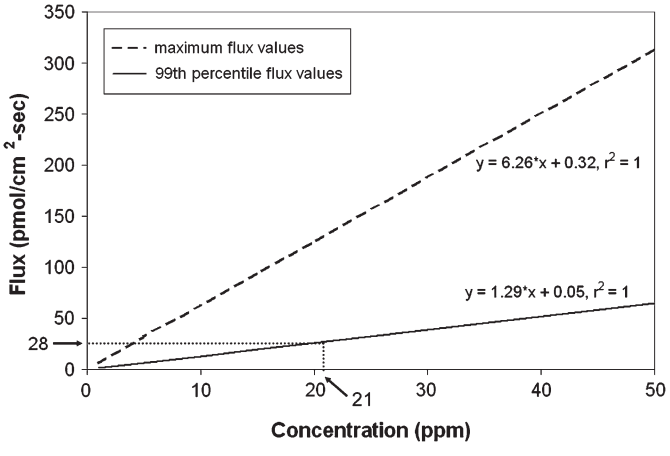

FIG. 6. Maximum and 99th percentile flux values in the human olfactory region predicted by the CFD model for H_2S exposure concentrations ranging from 1 to 50 ppm. An exposure concentration of 21 ppm is identified to correspond with a 99th percentile threshold flux value of 28 pmol/cm^2·s. Linear regression equations for the maximum and 99th percentile flux values are shown.

DISCUSSION

NE of H_2S in rats is a function of inspiratory flow rate, exposure concentration, and duration of exposure (Schroeter *et al.*, 2006). As airflow increased, time-averaged NE decreased due to the decreased residence time of the gas in the nasal cavity, and as exposure concentration increased, NE decreased due to presumably saturable uptake processes. To account for this nonlinear concentration dependence of NE with the rat nasal airflow model, a tissue phase was implemented to incorporate H_2S partitioning, diffusivity, and reaction kinetics. H_2S flux from the air phase was then intrinsically determined by the rate at which the hydrosulfide anion, HS^-, was cleared by diffusion and metabolism in nasal tissue. The first-order rate constant, k_f, and the Michaelis-Menten parameters V_{max} and K_m that govern systemic and metabolic clearance were estimated with a compartmental air-tissue PK model that shared a similar model structure with the CFD model of the rat nasal passages. These parameters were then implemented in the boundary condition defining H_2S mass transfer from the air phase in the CFD model, thereby utilizing the strengths of both well-mixed and distributed models in a PK-driven CFD approach.

Regional flux predictions from the PK-CFD model correlated well with the locations of H_2S-induced olfactory lesions in rat nasal passages, further indicating that olfactory lesion incidence is related to H_2S tissue dose. Since the number of regions in section 1 was not large enough to determine statistical significance, our analysis focused on section 2. At 30 and 80 ppm exposure concentrations, high lesion incidence occurred in distinct locations within olfactory epithelium and were generally associated with higher predicted flux values

(Fig. 4). There were also several locations (regions 4, 24, 27–29, and 32–33) that were predicted to receive high tissue flux but did not develop pathology following subchronic exposure to H_2S. These discrepancies are most likely attributable to site-specific metabolic factors or regional differences in tissue sensitivity to H_2S exposure, although numerical inaccuracies with the CFD model could also play a role.

There were also unaffected portions of the respiratory epithelium (e.g., parts of the lateral walls and the nasopharyngeal duct) that were predicted to receive high H_2S flux (Fig. 5). Acute exposures of rats to $\geq$ 80 ppm H_2S has been shown to induce respiratory epithelial regeneration on the lateral wall of the ventral meatus (Brenneman *et al.*, 2002). However, this pathology was not observed following 5 consecutive days of H_2S exposure to $\geq$ 80 ppm (Brenneman *et al.*, 2000), suggesting that rapid tissue regeneration of the respiratory epithelium may occur following acute H_2S exposure.

The primary mechanism for the toxic action of H_2S is hypothesized to be direct inhibition of cytochrome oxidase, an enzyme critical for mitochondrial respiration (Khan *et al.*, 1990; Nicholls and Kim, 1982, Dorman *et al.*, 2002). Decreased cytochrome oxidase acitivity was observed in the rat olfactory epithelium following an acute exposure to 80 ppm H_2S. Acute exposure to 400 ppm H_2S resulted in increased tissue sulfide concentrations and severe mitochondrial swelling in degenerating olfactory neurons, indicating that cytochrome oxidase inhibition is a likely mode of action for H_2S-induced olfactory pathology (Dorman *et al.*, 2002). Moreover, olfactory neuroepithelium is inherently more sensitive than nasal respiratory epithelium to H_2S-induced cytochrome oxidase inhibition. Therefore, the quantitative relationship between regional flux predictions and olfactory lesions (which were shown to be in accordance) was used to estimate H_2S toxicity levels in humans.

Olfactory mucosal lesions from the aforementioned H_2S subchronic inhalation study (Brenneman *et al.*, 2000) have been used as the critical effect by the U.S. Environmental Protection Agency to calculate an inhalation RfC. The RfC is an estimate of a continuous inhalation exposure to humans that is likely to be without appreciable risk of adverse effects over a person's lifetime (U.S. EPA, 1994). The current RfC for H_2S is 2×10^{-3} mg/m^3 (Integrated Risk Information System, http://www.epa.gov/iris, accessed June 2006), based on a NOAEL of 10 ppm (13.9 mg/m^3). To convert the NOAEL to a $NOAEL_{[HEC]}$, the RfC calculation relies on dosimetric adjustment factors that are used to account for species differences in delivered dose. Once a NOAEL is identified, an adjusted NOAEL, $NOAEL_{[ADJ]}$, is computed to convert to continuous exposure conditions (24 h/day for 70 years). This value is then multiplied by the regional gas dose ratio (RGDR) to obtain the $NOAEL_{[HEC]}$. The RGDR is a ratio of the relative minute volume to upper respiratory tract surface area ratios between the rat and the human and assumes complete extraction of the gas with a uniform dose throughout the upper respiratory tract. The current $NOAEL_{[HEC]}$ for H_2S is 0.64 mg/m^3 (~0.5 ppm) and was calculated by adjusting the time exposure of the subchronic inhalation study from 6 to 24 h and multiplying by the RGDR. The RfC was then determined by including uncertainty factors of 300 (a factor of 3 for interspecies extrapolation, 10 for sensitive populations, and 10 for subchronic exposure).

Although dosimetric adjustment factors consider differences in respiration and anatomy between species, they do not account for interspecies differences in regional airflow patterns, extraction efficiency, or metabolic clearance processes. H_2S is known to target the olfactory mucosa, which has a much larger relative surface area in rats than in humans (Fig. 1). The dorsal medial air stream provides a high volume of flow to the olfactory region in rats, which lines a complex series of ethmoturbinates that is very efficient at extracting chemicals from inhaled air (Kimbell *et al.*, 1997a). The human olfactory region, on the other hand, receives a low proportion of the total inhaled airflow and, subsequently, of any inhaled gas (Subramaniam *et al.*, 1998). CFD models can help identify and quantify these interspecies differences in airflow and uptake patterns to refine estimates of risk to human health.

TABLE 4
Comparison of Lesion Incidence and Threshold Flux Values (pmol/cm^2·s) in Section 2

	Exposure concentration (ppm)			Region numbers (concentration)
	10	30	80	
Highest flux/no lesions	34	65	126	2(10), 33(30), 32(80)
Lowest flux/lesions	NA	28	20	38(30), 31(80)

Note. NA, not applicable.

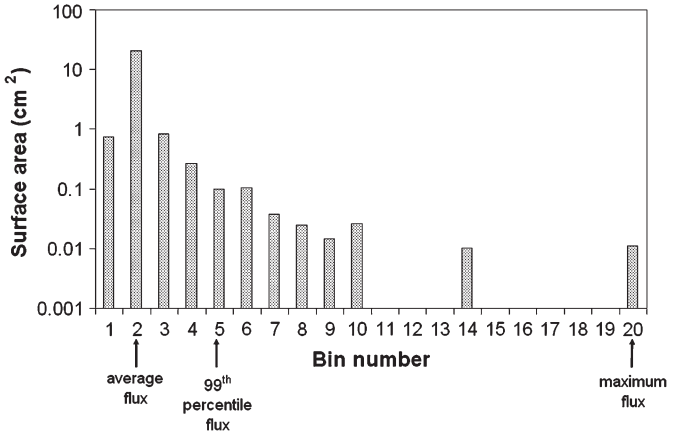

FIG. 7. Human olfactory surface area partitioned by predicted H_2S flux at a 21-ppm exposure concentration. The minimum flux was 0 (negative flux values were lumped into bin 1) and the maximum flux was 28 pmol/cm^2·s. Flux bins computed at other exposure concentrations between 1 and 50 ppm displayed a similar partitioning of olfactory surface area.

The PK-CFD model developed in this study was used to overcome the limitations of the simplifying interspecies adjustment factors by using flux predictions as a tissue dose surrogate to derive a more refined estimate of a $NOAEL_{[HEC]}$ for H_2S. Since olfactory lesion incidence and predicted flux values were in statistical concordance, the lesion data from section 2 (Table 3, Fig. 4) was used to estimate a flux measure that serves as a threshold value to lesion development.

Lesions were observed in regions 2, 16, 17, 21, and 37–39 with low to moderate (17–75%) incidence at 30 ppm (the lowest-observed-adverse effect level) and with moderate to high (75–100%) incidence at 80 ppm, indicating a clear concentration-response relationship at these locations. The maximum flux associated with the NOAEL (10 ppm) was 34 pmol/cm^2·s, occurring in region 2 (Table 4). Although this could be considered a threshold flux value since lesions were observed in this region with increased incidence at 30 and 80 ppm, respectively, this flux value was significantly greater than the remaining fluxes in section 2 at 10 ppm. In addition, there were several regions (17, 37–39) where lesions were observed with lower predicted fluxes at a 30-ppm exposure concentration. The minimum of these values was 28 pmol/cm^2·s, occurring in region 38 (Table 4). It should be noted that at 80 ppm, there was one region predicted to receive lower flux (20 pmol/cm^2·s) where lesions occurred. However, lesion incidence in this region did not exhibit a clear dependence on exposure concentration since there were no lesions observed at 30 ppm. For these reasons, 28 pmol/cm^2·s was selected as the threshold flux value.

Assuming that similar responses in olfactory epithelium will be seen in humans for equivalent flux values (i.e., equal tissue doses invoke similar responses in rats and humans), we can use this threshold flux value to estimate an equivalent human exposure concentration. The maximum and 99th percentile olfactory flux values predicted by the human nasal CFD model were computed at H_2S exposure concentrations ranging from 1 to 50 ppm (Fig. 6). Using a linear regression fit, we found that an H_2S exposure concentration of ~21 ppm will yield a 99th percentile olfactory flux value of 28 pmol/cm^2·s. Following the protocol used for the RfC derivation, the $NOAEL_{[HEC]}$ was then determined by adjusting for continuous exposure conditions, in this case from 6 to 24 h. The $NOAEL_{[HEC]}$ for H_2S was therefore estimated to be ~5 ppm (or 7.5 mg/m^3), a concentration usually associated with a noticeable odor of moderate intensity (Beauchamp *et al.*, 1984).

To examine how predicted fluxes were distributed across the olfactory region, the human olfactory surface area was partitioned into bins based on H_2S tissue flux. An individual flux bin represents the portion of the olfactory surface area that receives flux within a specified range (Kimbell *et al.*, 2001a). At an exposure concentration of 21 ppm, olfactory flux values from 0 to 28 pmol/cm^2·s were equally spaced into 20 partitions or bins (Fig. 7). The bin corresponding to the highest fluxes (bin 20) contained less than 0.05% of the total olfactory surface area, and bins 11–20 contained less than 0.1% of the olfactory surface area. Greater than 90% of the olfactory surface area occurred in bin 2, which is where the average olfactory flux occurred.

The 99th percentile flux values were selected to estimate the $NOAEL_{[HEC]}$ to account for the fact that only a very small portion of the human olfactory epithelium was predicted to receive the maximum flux and also to account for possible inaccuracies computing wall mass fluxes with the CFD model. Use of the 99th percentile flux value instead of the average flux value provided a more conservative risk estimate, while still capturing localized regions of high mass flux predicted by the CFD model. These high flux regions are evident on the anterior ventral margin of the right superior turbinate and the medial aspects of the right superior and middle turbinates (Fig. 5). The 95th percentile olfactory flux value was also considered for use in the risk estimate calculation; however, this resulted in estimated H_2S concentration levels (~10 ppm) that were above the tolerable threshold for continuous exposure conditions.

In summary, interspecies PK-CFD models provide a basis for extrapolating nasal lesion and extraction data in rats to estimate acceptable toxicity levels in humans. A refined estimate of a $NOAEL_{[HEC]} = 5$ ppm for H_2S was developed based on a conservative quantitative dosimetric approach rather than using default dosimetric assumptions for interspecies extrapolation. Metabolic parameters that were derived for the rat were scaled to human conditions based on an allometric scaling that was adjusted to account for the relative differences in nasal surface area between species. While there is currently no data to support this extrapolation, it was consistent with previous modeling efforts involving interspecies clearance extrapolations. This scaling parameter will be refined once H_2S extraction and metabolic processes are determined in other animal species (e.g., mouse).

ACKNOWLEDGMENTS

This study was funded in part by a grant from the American Forest and Paper Association and by the American Chemistry Council. We appreciate the comments of Harvey Clewell, Elizabeth Roberts, and Cecilia Tan during their review of the manuscript.

REFERENCES

Agency for Toxic Substances and Disease Registry (ATSDR) (1999). *Toxicological Profile for Hydrogen Sulfide.* U.S. Department of Commerce, Springfield, VA.

Beauchamp, R. O., Jr, Bus, J. S., Popp, J. A., Boreiko, C. J., and Andjelkovich, D. A. (1984). A critical review of the literature on hydrogen sulfide toxicity. *Crit. Rev. Toxicol.* **13,** 25–97.

Brenneman, K. A., James, R. A., Gross, E. A., and Dorman, D. C. (2000). Olfactory neuronal loss following subchronic inhalation exposure to low levels of hydrogen sulfide in adult male CD rats. *Toxicol. Pathol.* **28,** 326–333.

Brenneman, K. A., Meleason, D. F., Marshall, M. W., James, R. A., Gross, E. A., Martin, J. T., and Dorman, D. C. (2002). Nasal lesions following acute inhalation exposure of male CD rats to hydrogen sulfide: Reversiblity and the possible role of regional metabolic capacity in lesion distribution. *Toxicol. Pathol.* **30,** 200–208.

Dorman, D. C., Moulin, F. J. M., McManus, B. E., Mahle, K. C., James, R. A., and Struve, M. F. (2002). Cytochrome oxidase inhibition induced by acute hydrogen sulfide inhalation: Correlation with tissue sulfide concentrations in the rat brain, liver, lung, and nasal epithelium. *Toxicol. Sci.* **65,** 18–25.

Dorman, D. C., Struve, M. F., Gross, E. A., and Brenneman, K. A. (2004). Respiratory tract toxicity of inhaled hydrogen sulfide in Fischer-344 Rats, Sprague Dawley Rats, and B6C3F1 mice following subchronic (90-day) exposure. *Toxicol. Appl. Pharmacol.* **198,** 29–39.

Glass, D. C. (1990). A review of the health effects of hydrogen sulphide exposure. *Ann. Occup. Hyg.* **34,** 323–327.

Kepler, G. M., Richardson, R. B., Morgan, K. T., and Kimbell, J. S. (1998). Computer simulation of inspiratory nasal airflow and inhaled gas uptake in a rhesus monkey. *Toxicol. Appl. Pharmacol.* **150,** 1–11.

Keyhani, K., Scherer, P. W., and Mozell, M. M. (1997). A numerical model of nasal odorant transport for the analysis of human olfaction. *J. Theor. Biol.* **186,** 279–301.

Khan, A. A., Schuler, M. M., Prior, M. G., Yong, S., Coppock, R. W., Florence, L. Z., and Lillie, L. E. (1990). Effects of hydrogen sulfide exposure on lung mitochondrial respiratory chain enzymes in rats. *Toxicol. Appl. Pharmacol.* **103,** 482–490.

Kimbell, J. S., Godo, M. N., Gross, E. A., Joyner, D. R., Richardson, R. B., and Morgan, K. T. (1997a). Computer simulation of inspiratory airflow in all regions of the F344 rat nasal passages. *Toxicol. Appl. Pharmacol.* **145,** 388–398.

Kimbell, J. S., Gross, E. A., Joyner, D. R., Godo, M. N., and Morgan, K. T. (1993). Application of computational fluid dynamics to regional dosimetry of inhaled chemicals in the upper respiratory tract of the rat. *Toxicol. Appl. Pharmacol.* **121,** 253–263.

Kimbell, J. S., Gross, E. A., Richardson, R. B., Conolly, R. B., and Morgan, K. T. (1997b). Correlation of regional formaldehyde flux predictions with the distribution of formaldehyde-induced squamous metaplasia in F344 rat nasal passages. *Mutat. Res.* **380,** 143–154.

Kimbell, J. S., Overton, J. H., Subramaniam, R. P., Schlosser, P. M., Morgan, K. T., Conolly, R. B., and Miller, F. J. (2001a). Dosimetry modeling of inhaled formaldehyde: Binning nasal flux predictions for quantitative risk assessment. *Toxicol. Sci.* **64,** 111–121.

Kimbell, J. S., Subramaniam, R. P., Gross, E. A., Schlosser, P. M., and Morgan, K. T. (2001b). Dosimetry modeling of inhaled formaldehyde: Comparisons of local flux predictions in the rat, monkey, and human nasal passages. *Toxicol. Sci.* **64,** 100–110.

Krishnan, K., and Andersen, M. E. (1991). Interspecies scaling in pharmacokinetics. In *New Trends in Pharmacokinetics* (A. Rescigno and A. K. Thakur, Eds.), pp. 203–226. Plenum Press, New York.

Lopez, A., Prior, M., Yong, S., Lillie, L., and Lefebvre, M. (1988). Nasal lesions in rats exposed to hydrogen sulfide for four hours. *Am. J. Vet. Res.* **49,** 1107–1111.

Mahmood, I. (2001). Interspecies scaling of inhalational anesthetic potency minimum alveolar concentration (MAC): Application of a correction factor for the prediction of MAC in humans. *Am. J. Ther.* **8,** 237–241.

Mauderly, J. L. (1986). Respiration of F344 rats in nose-only inhalation exposure tubes. *J. Appl. Toxicol.* **6,** 25–30.

Mendenhall, W., Schaeffer, R. L., and Wackerly, D. D. (1981). *Mathematical Statistics with Applications.* Duxbury Press, Boston, MA.

Mordenti, J., and Chappell, W. (1989). The use of interspecies scaling in toxicokinetics. In *Toxicokinetics and New Drug Development.* (A. Yacobi, J. P. Skelly, and V. K. Batra, Eds.), p. 42. Pergamon Press, New York.

Moulin, F. J.-M., Brenneman, K. A., Kimbell, J. S., and Dorman, D. C. (2002). Predicted regional flux of hydrogen sulfide correlates with distribution of nasal olfactory lesions in rats. *Toxicol. Sci.* **66,** 7–15.

Nicholls, P., and Kim, J. K. (1982). Sulphide as an inhibitor and electron donor for the cytochrome c oxidase system. *Can. J. Biochem.* **60,** 613–623.

Ramsey, J. C., and Andersen, M. E. (1984). A physiologically based description of the inhalation pharmacokinetics of styrene in rats and humans. *Toxicol. Appl. Pharmacol.* **73,** 159–175.

Reiffenstein, R. J., Hulbert, W. C., and Roth, S. H. (1992). Toxicology of hydrogen sulfide. *Annu. Rev. Pharmacol. Toxicol.* **32,** 109–134.

Roberts, E. S., Wong, V. A., McManus, B. E., Marshall, M. W., Lancianese, S., and Dorman, D. C. (2006). Changes in intracellular pH play a secondary role in hydrogen sulfide-induced nasal cytoxicity. *Inhal. Toxicol.* **18,** 159–167.

Scherer, P. W., Keyhani, K., and Mozell, M. M. (1994). Nasal dosimetry modeling for humans. *Inhal. Toxicol.* **6**(Suppl), 85–97.

Schroeter, J. D., Kimbell, J. S., Bonner, A. M., Roberts, K. C., Andersen, M. E., and Dorman, D. C. (2006). Incorporation of tissue reaction kinetics in a computational fluid dynamics model for nasal extraction of inhaled hydrogen sulfide in rats. *Toxicol. Sci.* (in press).

Subramaniam, R. P., Richardson, R. B., Morgan, K. T., Guilmette, R. A., and Kimbell, J. S. (1998). Computational fluid dynamics simulations of inspiratory airflow in the human nose and nasopharynx. *Inhal. Toxicol.* **10,** 91–120.

U.S. Environmental Protection Agency (U.S. EPA) (1994). *Methods for Derivation of Inhaled Reference Concentrations and Application of Inhalation Dosimetry.* Office of Research and Development, Washington, DC. EPA/600/8-90-066F.